J Electroceram (2007) 18:261–268
DOI 10.1007/s10832-007-9124-4

# Effect of Cr additions on the microstructural stability of Ni electrodes in ultra-thin $BaTiO_3$ multilayer capacitors

**Anton V. Polotai · Tae-Hee Jeong · Gai-Ying Yang · Elizabeth C. Dickey · Clive A. Randall · Pascal Pinceloup · Abhijit S. Gurav**

Received: 5 February 2007 / Accepted: 29 March 2007 / Published online: 19 April 2007


**Abstract** Microstructural control in thin-layer multilayer ceramic capacitors (MLCC) is one of the present day challenges to maintain an increase in capacitive volumetric efficiency. This present paper opens a series of investigations aimed to engineer the stability of ultra-thin Ni electrodes in $BaTiO_3$-based multilayer capacitors using refractory metal additions to Ni. Here, pure Ni and Ni–1 wt.% Cr alloy powders are used to produce 0805-type BME MLCCs with 300 active layers and with dielectric and electrode layer thickness around 1 μm. To investigate the continuity of Ni electrodes, both MLCC chips with pure and doped electrodes were sintered at different temperatures for 5 h. It is found that the continuity of Ni electrodes is improved most likely due to the effect of Cr on the low-melting point (Ni,Ba,Ti) interfacial alloy layer formation. The interfacial alloy layer is not observed when Cr is segregated at Ni-$BaTiO_3$ interface in the Cr-doped samples, while it is found in all undoped samples. The interfacial alloy layer is believed to increase mass-transfer along the Ni-$BaTiO_3$ interfaces facilitating an acceleration of Ni electrodes discontinuities.

**Keywords** MLCC · Nickel electrodes · $BaTiO_3$ · Ni-$BaTiO_3$ interfaces

A. V. Polotai (✉) · T.-H. Jeong · G.-Y. Yang · E. C. Dickey · C. A. Randall
Center for Dielectric Studies, Department of Materials Science and Engineering, The Pennsylvania State University, University Park, PA 16802, USA
e-mail: avp10@psu.edu

P. Pinceloup · A. S. Gurav
KEMET Electronics Corporation, P.O. Box 849, Fountain Inn, SC 29644, USA

## 1 Introduction

The ever-increasing demand for high-performance, high-volumetric efficiency and high-reliability multilayer ceramic capacitors (MLCCs) offers a variety of challenges to the capacitor industry in the areas of particulate materials, dielectric compositions and manufacturing technology [1, 2]. Currently, one of the main problems arising in the processing of ultra-thin, base-metal electrode MLCCs with dielectric and electrode layer thicknesses around 1 μm or less is the microstructural evolution of the electrode layers during co-sintering which leads electrode discontinuities [3]. This generates a number of problems including electrical shorts, lower capacitance, modifies profile of devices and decreased reliability. Thus, the understanding and control of the forces that drive instabilities in multilayer structures is of major technological importance to high capacitance components.

In general, the electrode microstructural evolution and interfacial reactions that take place during material processing have to be considered from both thermodynamic driving forces and kinetic factors. Broadly speaking, there are three main thermodynamic driving forces that can affect layering stability at high temperatures: energy of mixing between the layer materials, elastic strain energy, and relative interfacial to grain boundary free energies [4–10]. Generally, the free energy of the multilayer can be reduced through interdiffusion between layers or morphological evolution to non-planar or discontinuous interfaces. This problem is now becoming a major technical challenge as layers approach sub-micron length scales in MLCCs. To date, there is no clear explanation of which mechanisms dominate and lead to electrode discontinuities in ultra-thin Ni-$BaTiO_3$ based MLCCs.

Considering the above-mentioned driving forces, one possible driving force for morphological instabilities in multilayer systems is the reduction of elastic strain energy, which can arise from numerous sources, including mismatches in lattice constants, thermal expansion coefficients, or elastic constants between the layers [5, 10, 11]. The main contribution to the elastic stresses in MLCCs arises from the mismatch of densification rates between the ceramic layers and metal electrodes during co-sintering [7, 8]. Local variations in elastic stress take place when perturbations in layer thickness appear [7], which are unavoidable in polycrystalline systems such as MLCCs. Such stress gradients drive mass transport from the thinnest areas, where stresses are highest, to the thickest parts of the same layer, where stresses are lowest. This diffusion leads to growth of perturbations and instability of layering.

Polycrystalline layers add another complexity, and the relative ratio of the grain boundary to interfacial free energies per unit area, $\gamma_{gb}/\gamma_{int}$, can lead to capillary instabilities and is therefore an additional controlling factor in the morphological stability of the multilayer [4, 6, 12, 13]. Figure 1 outlines the case of polycrystalline multilayered A–B materials in which there is an equilibrium groove angle at the point where B–B grain boundary meets two A–B interfaces. This groove angle is determined by the ratio of grain boundary to interfacial free energies $\gamma_{gb}/\gamma_{int}$ through Eq. 1 [8],

$$2\cos\theta = \gamma_{gb}/\gamma_{int} \quad (1)$$

where $\theta$ is half of the angle between two A–B interfaces. While this model ignores anisotropy in the interfacial and grain boundary free energies, it is still a useful framework in which to understand morphological stability of layered materials. When $\gamma_{gb}/\gamma_{int}$ is large, i.e. $\gamma_{int}$ is relatively small, significant grooving occurs to maximize the interfacial area relative to the grain boundary area, thus lowering the total free energy of the system. Sufficiently large values of $\gamma_{gb}/\gamma_{int}$ result in deep groves, which can lead to layer pinch-off and an unstable microstructure. Note that this interfacial thermodynamic argument is contrary to the situation of a thin film on free surface in which low interfacial energies (relative to surface free energies) generally are desirable for enhanced wettability.

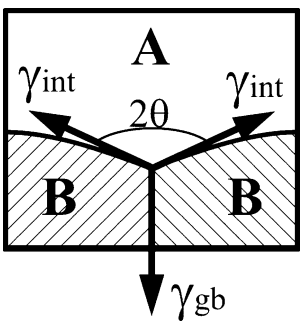


**Fig. 1** Schematic view of a grain boundary groove after reference [8]

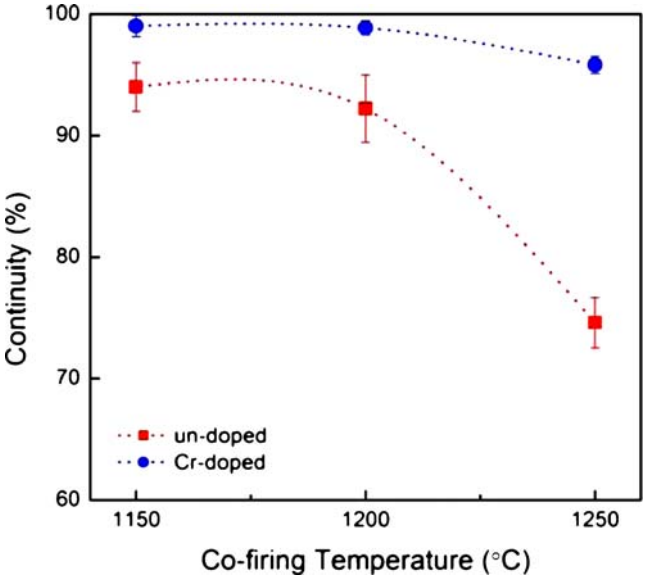


**Fig. 2** Continuity of Ni electrodes in Ni-$BaTiO_3$ MLCCs after co-firing at different temperatures for 5 h

If the layers are unstable to the capillary forces and develop grooves, they will ultimately pinch off and lead to layer breakup. The kinetics of this process depend on interfacial and grain boundary diffusivities as well as the layer thickness. Studies on the Au–Cu microlaminate system showed that the groove growth rate for this system was independent of absolute laminate layer thickness, however thinner layers reached breakdown sooner [12].

In addition to the morphological and microstructural considerations discussed above, the chemical stability of the interfaces is also important to the overall multilayer integrity. Considering the chemical energy of mixing, when layered systems contain elements with positive heats of mixing ($\Delta H_{mix}$), they are immiscible and no intermixing will occur [7]. When $\Delta H_{mix}<0$, solid solutions or compounds can form and may destroy layering. In the case of Ni and $BaTiO_3$, the $\Delta H_{Ni-Ba}\sim+1$ kJ/g, whereas $\Delta H_{Ni-Ti}\sim-140$ kJ/g [14, 15]. Therefore, alloying is thermodynamically possible if $BaTiO_3$ undergoes significant reduction [16–19]. In fact, we recently identified the formation of discrete interfacial alloy layers consisting of Ni, Ba and Ti with a thickness of 5–15 nm between Ni electrodes and $BaTiO_3$ in commercial MLCCs [16–19]. The appearance of this alloy was attributed to the local reduction of the $BaTiO_3$ by residual carbon remaining from the binder burnout process. It was also concluded that the nickel acts as a catalysts to promote this reaction. Phase diagram calculations confirmed that a (Ni,Ba,Ti) alloy could form a liquid phase at temperatures as low as 1,150°C, whereas a common sintering temperature for the Ni-$BaTiO_3$

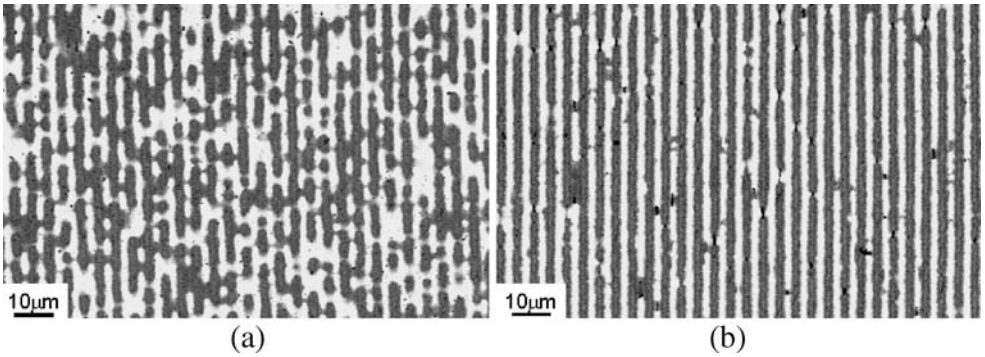


**Fig. 3** VC-SEM images of MLCC with pure (**a**) and Cr-doped (**b**) Ni electrodes, co-fired at 1,250°C for 5 h

MLCC processing is around 1,250–1,300°C [3]. The presence of the high-temperature interfacial liquid phase could modify the interfacial free energy and provide a fast kinetic pathway for mass transport which leads to the enhanced Ni grain growth and Ni layers degradation.

This paper reports the effects of Cr additions to the Ni electrodes on the multilayer microstructural evolution and interfacial reactions during co-sintering in conditions typical of those encountered in MLCC production. Chromium is a well known nickel additive [20–22]. It has a much higher melting temperature ($Tm_{Cr}$=1,857°C) compared to Ni ($Tm_{Ni}$=1,453°C) and a negative enthalpy of mixing with Ni and Ti. Also, Ni–Cr alloys are commonly used for high-temperature structural and electrical applications. The effect of Cr on the Ni electrode continuity and, especially, on the MLCC's electrical properties is difficult to predict. While Cr has a very high affinity to oxygen ($\Delta H_{ox}$=−1,135 kJmol) and could reduce the Ni-$BaTiO_3$ interfacial free energy leading to lower contact resistance

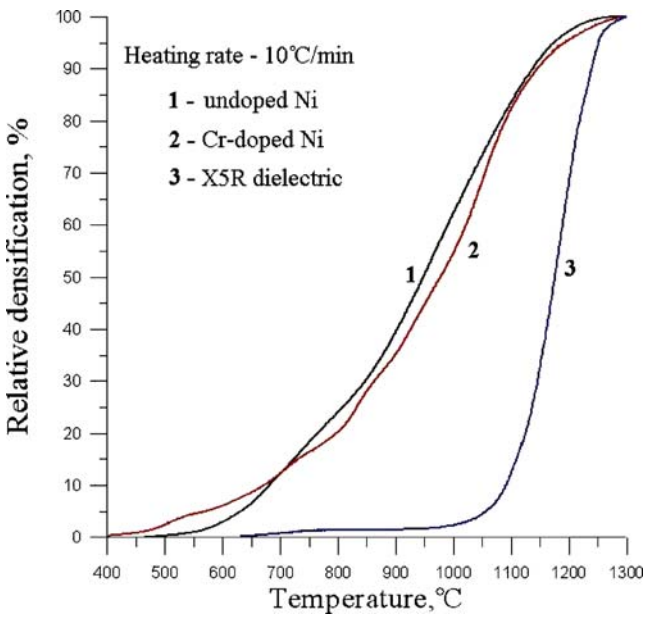


**Fig. 4** Comparison of sintering kinetics for undoped and Cr-doped Ni electrode materials as well as the $BaTiO_3$ based dielectric material

[23–25], the addition of Cr to Ni has also been reported to decrease the grain boundary energy [26], which could result in the improvement of Ni layers stability due to the reduction of $\gamma_{gb}/\gamma_{int}$ ratio. To help elucidate the role of Cr on interface chemistry and improved electrode stability, we perform microstructural and microchemical analyses by transmission electron microscopy (TEM) and electron energy loss spectroscopy (EELS). The effect of Cr addition on the electrical properties will be discussed in a following paper (Polotai, unpublished).

## 2 Experimental procedures

0805-type MLCC green chips (1.60×0.87×0.90 mm, with 300 dielectric layers) were manufactured by KEMET Electronic Corporation, Greenville, SC, USA. Two types of MLCC samples, one with undoped Ni electrodes and another with 1 wt.% Cr-doped Ni electrodes were prepared by conventional tape casting techniques. The Ni–1 wt.% Cr alloy powder for this study was made by a flame-gas phase method. The thickness of electrode and dielectric layers were 0.9 and 1.2 μm respectively. The dielectric was a $BaTiO_3$-based X5R-type material, which was formulated with chemical additives such as $Y_2O_3$ and MnO. For binder burnout, the green chips were held at 220–280°C for 20–30 h in a $N_2$–$O_2$ atmosphere. Next, the green chips were co-fired in the temperature range from 1,150 to 1,250°C for 5 h in a reducing atmosphere using an $H_2O$–$N_2$–$H_2$ gas mixture with $pO_2$ level from $10^{-9}$ to $10^{-11}$ atm at peak temperature. The co-fired Ni-$BaTiO_3$ MLCCs were then re-oxidized using an atmosphere with $pO_2$ level from $10^{-8}$ to $10^{-9}$ atm for 3 h at temperature range from 900 to 1,100°C.

To investigate the shrinkage behavior of undoped and Cr-doped Ni electrode materials as well as the $BaTiO_3$-based dielectric material, small pellets (6×2 mm) were uniaxially pressed from corresponding dielectric and electrode pastes and then sintered using a precise rate-controlled high-temperature dilatometer equipped with a

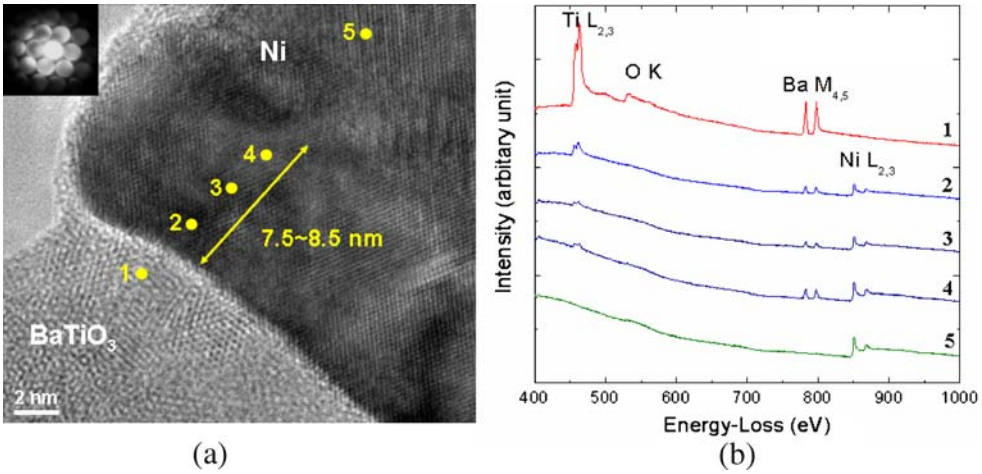


**Fig. 5** HR-TEM image (**a**) and corresponding EEL spectra (**b**) for MLCC with undoped Ni electrodes, co-fired at 1,250°C for 5 h

gas control system [27]. All samples were non-isothermally sintered at a 10°C/min heating rate in a reducing atmosphere ($pO_2 \sim 10^{-9}$–$10^{-11}$ atm at peak temperature).

The sintered MLCC samples were characterized by voltage contrast-scanning electron microscopy (VC-SEM), high resolution-transmission electron microscopy (HR-TEM), energy dispersive X-ray spectroscopy (EDS) and electron energy loss spectroscopy (EELS). VC-SEM imaging was performed using a HITACHI S-3000H SEM operated with an accelerating voltage of 2.5 kV and a DC field of 7 V applied across the MLCC electrodes. In the VC-SEM mode, the negatively biased electrodes are brighter than the surrounding area and allow better observation of imperfections in the electrode and dielectric layers. If there is a discontinuous region in the electrode, that area appears dark in the VC-SEM image obtained by a negative polarity [Fig 2(b)]. The microstructure and microchemistry of the dielectric-electrode interfaces were analyzed using a JEOL-2010 field-emission TEM operated at 200 kV, equipped with Gatan Enfina EEL spectrometer and an Oxford Systems EDS detector. A low-background beryllium Gatan double-tilt holder was used to reduce the production of spurious X-rays. The HR-TEM images of the interfaces between Ni and $BaTiO_3$ were recorded with a Gatan CCD camera.

**Table 1** Chemical composition and thickness of interfacial layers between Ni and $BaTiO_3$ at different co-firing temperatures.

| Co-firing temperature, °C | Ni, mol% | Ti, mol% | Ba, mol% | Thickness, nm |
|---|---|---|---|---|
| 1,150 | 96.1± 9.0 | 1.5± 1.0 | 2.5± 2.0 | 5.8±1.4 |
| 1,200 | 94.9± 8.4 | 2.1± 1.4 | 3.0± 0.8 | 6.5±1.5 |
| 1,250 | 92.4± 8.2 | 3.7± 1.9 | 3.9± 1.3 | 8.0±1.5 |

The continuity of the Ni electrodes was quantified based on measurements from the VC-SEM images. The total length of the electrode and the lengths of imperfections were measured and normalized for each VC-SEM image. Average values and standard deviations were calculated from more than five VC-SEM images for each MLCC sample.

## 3 Results and discussion

Investigation of the Ni electrode continuity shows that the sintering temperature as well as the electrode chemistry affects the stability of the internal electrodes. Figure 2 quantifies the continuity of samples held at 1,150, 1,200 and 1,250°C at peak temperature for 5 h. As sintering temperature increases, the electrodes become more discontinuous for both undoped and Cr-doped Ni MLCCs. The continuity of Ni electrodes decreases non-linearly with increasing sintering temperature. However, the Cr-doped samples show a much higher level of electrode stability than undoped samples. Figure 3 shows the VC-SEM images of MLCC samples with undoped and Cr-doped Ni electrodes co-fired at 1,250°C for 5 h. It can be seen that the addition of 1 wt.% of Cr to Ni significantly improves the continuity of 0.9 μm thick electrodes in these multilayers. The fact that the continuity begins to decrease in the Cr-doped electrodes at 1,250°C suggests that the electrodes remain thermodynamically unstable to morphological instabilities, but that the kinetics of the process are dramatically decreased in these samples.

To determine if the Cr additions affect the densification rate of Ni electrodes, thus changing the magnitude of the internal stresses in the multilayer system during co-firing, a comparison of sintering kinetics for undoped and Cr-doped Ni electrode materials as well as for the $BaTiO_3$-based

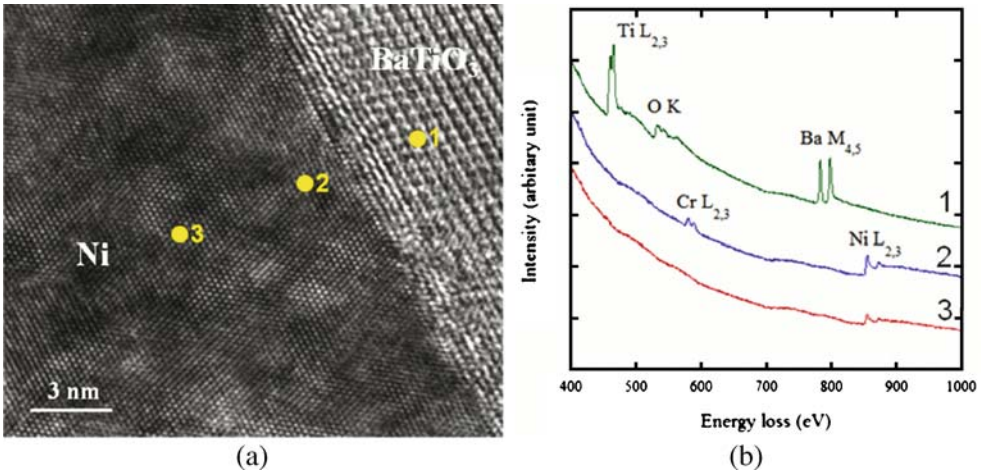


**Fig. 6** HR-TEM image (**a**) and corresponding EEL (**b**) spectra for the Ni-$BaTiO_3$ interface with Cr segregation

dielectric material was carried out by dilatation experiments (Fig. 4). The undoped and Cr-doped Ni pellets produced from the corresponding electrode inks showed very similar densification curves compared to the dielectric material. The similar densification behaviors of both Cr-doped and unmodified Ni indicate that the level of elastic strain energy generated during sintering will be quite similar for both types of electrode materials, so the differences in the electrode stability cannot be attributed to differences in internal stresses.

The microstructure and microchemistry of the Ni-$BaTiO_3$ interfaces in undoped and Cr-doped MLCCs were analyzed by HR-TEM with EDS and EELS. Figure 5 shows a typical HR-TEM image and corresponding EEL spectra for the Ni-$BaTiO_3$ interface of an undoped MLCC sintered at 1,250°C for 5 h. Shown in Fig. 5(a) is an edge-on Ni-$BaTiO_3$ interface obtained with the incident electron beam parallel to the <110> zone axis of Ni and the insert is a nanodiffraction pattern taken from the layer. As indicated by the arrow in Fig. 5(a), a significant change in image contrast is observed in Ni near the interface, suggesting the presence of an interfacial layer about 8 nm thick [17]. Moiré fringes are apparent in the Ni electrode region, which is most likely due to surface oxidation of the Ni, while they are absent in the interface region. The appearance of a coherent (Ni,Ba,Ti) alloy at the interface is confirmed by high resolution TEM technique and EELS analysis [Fig. 5(b)]. EEL spectra 2, 3 and 4, acquired from the interfacial layer, exhibit a Ni $L_{2,3}$ edge along with Ti $L_{2,3}$ and Ba $M_{4,5}$ edges without an O K edge. These results are consistent with our previous observations from numerous Ni-$BaTiO_3$ MLCC samples. [16–18].

The chemical composition of the interface layer in undoped specimens as function of sintering temperature was determined though quantification of EEL spectra and is presented in Table 1 together with measured layer thicknesses. These values are also in good agreement with those obtained by Yang at al. [17]. Within the experimental errors, the interface layer composition and its thickness are mostly independent of the sintering temperature.

A different situation was observed in multilayer capacitors with Cr additions to the Ni electrodes. Two different

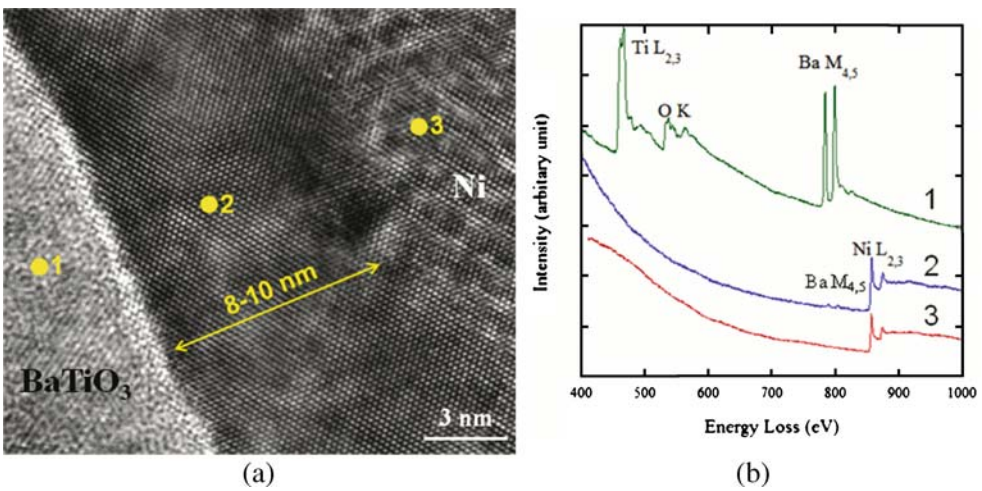


**Fig. 7** HR-TEM image (**a**) and corresponding EEL (**b**) spectra for the Ni-$BaTiO_3$ interface without Cr segregation

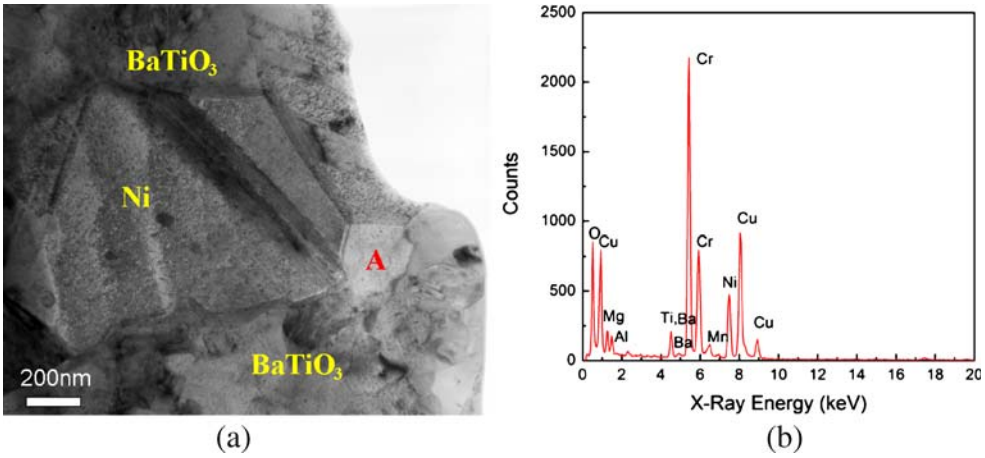


**Fig. 8** TEM bright field image (**a**) and corresponding EDS spectrum (**b**) from region A for Cr-doped samples co-fired at 1,250°C for 5 h

types of Ni-$BaTiO_3$ interfaces were found in Cr-doped samples sintered at 1,250°C for 5 h: (1) interfaces with Cr segregation and without the formation of interfacial alloy layer; (2) interfaces without Cr segregation and with the formation of interfacial alloy layer. The appearance of two types of interfaces is attributed to inhomogeneous Cr distributions in the original Ni paste used in the MLCC production. Figure 6 shows a typical HR-TEM image and corresponding EEL spectra for the Ni-$BaTiO_3$ interface with Cr segregation. Where the Cr segregates at the interface, the Moiré fringes are apparent in the entire Ni electrode region up to the interface with $BaTiO_3$ [Fig. 6(a)]. Figure 6(b) shows a corresponding EEL spectrum acquired from the electrode adjacent to the interface with $BaTiO_3$, which contains only Cr $L_{2,3}$ and Ni $L_{2,3}$ edges. The corresponding composition is approximately 6.8 at.% Cr and 93.2 at.% Ni. The spectrum does not show the coexistence of Ti $L_{2,3}$ and Ba $M_{4,5}$, which are indicative of the high-temperature liquid alloy phase present in undoped MLCCs.

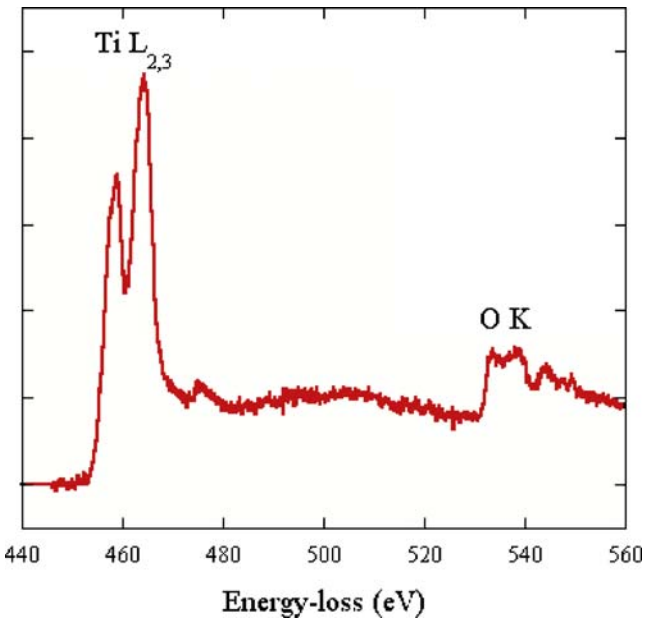


**Fig. 9** The EEL spectrum obtained from $BaTiO_3$ grains adjacent to Ni-$BaTiO_3$ interface in Cr-doped samples, which shows the existence of the reduced $Ti^{3+}$ ions

On the other hand, in electrode regions where Cr is not detected the typical interfacial Ni(Ti,Ba) alloy is formed between Ni and $BaTiO_3$, as shown in Fig. 7(a, b). The HRTEM image in Fig. 7(a) shows the alloy layer with ~ 8–10 nm thickness. The EELS data from position 2 in the alloy indicates a Ba-rich alloy with little to no evidence of the Ti $L_{2,3}$ edge. The corresponding composition is approximately 2 at.% Ba and 98 at.% Ni.

The exact mechanism by which Cr segregation suppresses the formation of the interfacial Ni(Ba,Ti) alloy is not clear at this point. Most likely, the Cr addition suppresses the carbon driven reduction of $BaTiO_3$ to the metallic states preventing the formation of the interfacial alloy layer. The appearance of the Ni $L_{2,3}$ edge together with the Cr $L_{2,3}$ edge on the EEL spectrum [Fig. 6(b), position 2] without Ba $M_{4,5}$ and Ti $L_{2,3}$ edges confirms this hypothesis. According to the thermodynamic calculation made by Yang et al. [17], the severe reduction of $BaTiO_3$ was caused by the oxidation of residual internal carbon, which was catalyzed by the Ni. So, it is possible that the Cr segregation at the Ni-$BaTiO_3$ interface may reduce the catalytic activity of Ni and prevent the reduction of $BaTiO_3$ into metallic Ba and Ti. Although the exact mechanism is unclear, there remains a clear experimental correlation between Cr segregation and the suppression of the high-temperature liquid Ni(Ba,Ti) interfacial phase formation. Obviously, the interfacial diffusion kinetics as well as the Ni electrode degradation kinetics would be much slower in the absence of this liquid phase.

Cr was also found in other regions other than the Ni-$BaTiO_3$ interface. First, Cr was detected inside some of $BaTiO_3$ grains adjacent to the Ni-$BaTiO_3$ interfaces. Cr to Ti substitution in $BaTiO_3$ unit cell is possible due to the similar ionic size between $Cr^{3+}$ and $Ti^{4+}$ ions ($R^{3+}_{Cr}$ =

0.615 nm, $R_{Ti}^{4+}$=0.605 nm) and behave as an acceptor [28]. Second, Cr was found as a separate Cr-rich phase distributed at the Ni-$BaTiO_3$ interfaces (Fig. 8). The EDS analysis of this Cr-rich phase revealed that the O $K_\alpha$ peak was shown together with the Cr and Ni peaks. This suggests that metallic Cr, with a strong affinity to oxygen, diffused from the Ni toward $BaTiO_3$ and formed oxides such as $Cr_2O_3$ at the Ni-$BaTiO_3$ interfaces [14, 15]. The Gibbs free energy for the formation of $Cr_2O_3$ (−738.1 kJ/mol) is much larger than for NiO (−101.3 kJ/mol) at 1,200°C, so it is believed that this new phase is $Cr_2O_3$ [29].

Another important finding is that the $BaTiO_3$ grains adjacent to Ni-$BaTiO_3$ interfaces were found to be oxygen deficient in the Cr-doped sample as compared to the undoped samples even through of the typical re-oxidation treatment was performed. The EEL spectrum (Fig. 9), collected from the $BaTiO_3$ grain adjacent to the Ni(Cr)-$BaTiO_3$ interface [Fig. 6(a), position 1], shows minor splitting of Ti $L_{2,3}$ edge and suppressed intensity of O K edges. This generally corresponds to the reduction of $Ti^{4+}$ ions to $Ti^{3+}$ state [16–18]. The lack of peak splitting in the Ti–$L_{2,3}$ edges for the reduced $BaTiO_3$ sample indicates a perturbation in the Ti–O octahedral coordination within the $BaTiO_3$ lattice due to oxygen deficiency [16, 18]. This modified EEL spectrum (Fig. 9) corresponds approximately to the $BaTiO_{2.70}$. Since the Cr has much higher affinity to oxygen compared to Ni and Ti, −1,135, −240 and −944 kJ/mol respectively [29], it can work as a sink for oxygen ions. The $Cr_2O_3$ phases, found at the Ni-$BaTiO_3$ interface [Fig. 8(a)], could be formed by oxygen taken from $BaTiO_3$ unit cell, which facilitates the formation of $Ti^{3+}$ ions.

## 4 Conclusions

It is shown that one of the main reasons for discontinuity of Ni electrodes in ultra-thin Ni-$BaTiO_3$ multilayer capacitors is the formation of liquid (Ni.Ba,Ti) alloy layer at Ni-$BaTiO_3$ interfaces. The presence of the high-temperature interfacial liquid phase modifies the interfacial free energy and provides a fast kinetic pathway for mass transport which leads to the enhanced Ni grain growth and Ni layers degradation. The formation of liquid alloy layer could be managed via the addition of refractory metals to Ni. The addition of Cr to Ni electrodes shows dual effects on the microstructure of Ni-$BaTiO_3$ interfaces. On the one hand, Cr suppresses the formation of the high-temperature interfacial liquid (Ni,Ba,Ti) alloy layer which significantly slows the discontinuity evolution in Ni electrodes. The interfacial alloy layer was not observed in the case of Cr segregation at the Ni-$BaTiO_3$ interfaces, while it was found at all Cr-free interfaces. On the other hand, Cr was found to diffuse into the $BaTiO_3$ grains, potentially acting as an acceptor. Moreover, the oxidation of Cr to $Cr_2O_3$ at the Ni-$BaTiO_3$ interface also facilitates the formation of additional amount of oxygen vacancies in adjacent $BaTiO_3$ grains. The high concentration of oxygen vacancies near the metal-dielectric interface may have a dramatic effect on the interfacial contact resistance [25, 30] and this will be discussed in a following paper (Polotai, unpublished).

**Acknowledgments** The authors acknowledge members of the NSF Industry/University Cooperative Research Centers Program Center for Dielectric Studies and the Materials Characterization Laboratory at Pennsylvania State University. This work was supported by the National Science Foundation, as part of the Center for Dielectric Studies under Grant No. 0120812.

## References

1. C.A. Randall, J. Ceram. Soc. Jpn. **109**, S2 (2001)
2. H. Nagata, S.W. Ko, E. Hong, C.A. Randall, S. Trolier-McKinstry, J. Am. Ceram. Soc. **89**, 2816 (2006)
3. H. Kishi, Y. Mizuno, H. Chazono, Jpn. J. Appl. Phys. Part 1 **42**, 1 (2003)
4. D. Josell, W.C. Carter, J.E. Bonevich, Nanostruct. Mater. **12**, 387 (1999)
5. N. Junqua, J. Grilhe, Philos. Mag., A, Phys. Condens. Matter, Struct. Defects Mech. Prop. **71**, 1125 (1995)
6. L. Klinger, Defect and Diffusion Forum **216**, 197 (2003)
7. A.C. Lewis, D. Josell, T.P. Weihs, Scr. Mater. **48**, 1079 (2003)
8. A.C. Lewis, A.B. Mann, D.V. Heerden, D. Josell, T.P. Weihs, Mater. Res. Soc. Symp. **652**, Y.1.3.1 (2001)
9. K.T. Miller, F.F. Lange, D.B. Marshall, J. Mater. Res. **5**, 151 (1990)
10. N. Sridhar, J.M. Rickman, D.J. Srolovitz, J. Appl. Physi. **82**, 4852 (1997)
11. N. Sridhar, J.M. Rickman, D.J. Srolovitz, Acta Mater. **45**, 2715 (1997)
12. H.L. Knoedler, G.E. Lucas, Metall. Mater. Trans. A. **34A**, 1043 (2002)
13. A. Misra, R.G. Hoagland, H. Kung, Philos. Mag. **84**, 1021 (2004)
14. D.P. Cann, C.A. Randall, J. Appl. Physi. **80**, 1628 (1996)
15. D.P. Cann, C.A. Randall, IEEE Trans. Ultrason. Ferroelectr. Freq. Control. **44**, 1405 (1997)
16. G.Y. Yang, E.C. Dickey, C.A. Randall, D.E. Barber, P. Pinceloup, M.A. Henderson, R.A. Hill, J.J. Beeson, D.J. Skamser, J. Appl. Physi. **96**, 7492 (2004)
17. G.Y. Yang, S.I. Lee, Z.J. Liu, C.J. Anthony, E.C. Dickey, Z.K. Liu, C.A. Randall, Acta Mater. **54**, 3513 (2006)
18. G.Y. Yang, G.D. Lian, E.C. Dickey, C.A. Randall, D.E. Barber, P. Pinceloup, M.A. Henderson, R.A. Hill, J.J. Beeson, D.J. Skamser, J. Appl. Physi. **96**, 7500 (2004)
19. G.Y. Yang, E.C. Dickey, C.A. Randall, M.S. Randall, L.A. Mann, J. Appl. Physi. **94**, 5990 (2003)
20. H. Hero, E. Sorbroden, J. Gjonnes, J. Mater. Sci. **22**, 2542 (1987)
21. F.G. Hodge, R.W. Kirchner, Corrosion **32**, 332 (1976)
22. E. Schippel, Thin Solid Films, **146**, 133 (1987)
23. P. Kritsalis, L. Coudurier, N. Eustathopoulos, J. Mater. Sci. **26**, 3400 (1991)
24. P. Kritsalis, V. Merlin, L. Coudurier, N. Eustathopoulos, Acta Metall. **40**, 1167 (1992)

25. D.P. Cann, J.P. Maria, C.A. Randall, J. Mater. Sci. **36**, 4969 (2001)
26. L.E. Murr, *Interfacial Phenomena in Metals and Alloys*. (Addison Wesley Publishing Company, New York, 1975)
27. A.V. Polotai, K.M. Breece, E.C. Dickey, C.A. Randall, A.V. Ragulya, J. Am. Ceram. Soc. **88**, 3008 (2005)
28. H.W. Jaffe, *Crystal Chemistry and Refractivity*. (Dover Publications Inc, Mineola, 1996)
29. C.H.P. Lupis, *Chemical Thermodynamics of Materials*. (Elsiver Science Publishing Co. Inc., New York, 1983)
30. E.H. Rhoderick, R.H. Williams, *Metal-Semiconductor Contacts*, 2nd edn. (Clarendon Press, Oxford, 1988)